



Multiple constrained minimum variance beamformer (MCMV) performance in connectivity analyses



Adonay S. Nunes ^{a,*}, Alexander Moiseev ^b, Natalia Kozhemiako ^{a,**}, Teresa Cheung ^c, Urs Ribary ^{b,d,e,f}, Sam M. Doesburg ^{a,b}

^a Biomedical Physiology and Kinesiology, Simon Fraser University, Burnaby, BC, Canada

^b Behavioral & Cognitive Neuroscience Institute, Simon Fraser University, Burnaby, BC, Canada

^c School of Engineering Science, Simon Fraser University, Burnaby, BC, Canada

^d Department Pediatrics and Psychiatry, University of British Columbia, Vancouver, BC, Canada

^e B.C. Children's Hospital Research Institute, Vancouver, BC, Canada

^f Department Psychology, Simon Fraser University, Burnaby, BC, Canada

ABSTRACT

Functional brain connectivity is increasingly being seen as critical for cognition, perception and motor control. Magnetoencephalography and electroencephalography are modalities that offer noninvasive mapping of electrophysiological interactions among brain regions, yet suffer from signal leakage and signal cancellation when estimating brain activity. This leads to biased connectivity values which complicate interpretation. In this study, we test the hypothesis that a Multiple Constrained Minimum Variance beamformer (MCMV) outperforms the more traditional Linearly Constrained Minimum Variance beamformer (LCMV) for estimation of electrophysiological connectivity. To this end, MCMV and LCMV performance is compared in task related analyses with both simulated data and human MEG recordings of visual steady state signals, and in resting state analyses with simulated data and human MEG data of 89 subjects. In task related scenarios connectivity was estimated using coherence and phase locking values, whereas envelope correlations were used for the resting state data. We also introduce a novel Augmented Pairwise MCMV (APW-MCMV) approach for signal leakage suppression in resting state analyses and assess its performance against LCMV and more conventional MCMV approaches. We demonstrate that with MCMV effects of signal mixing and coherent source cancellation are greatly reduced in both task related and resting state conditions, while in contrast to other approaches 0- and short time lag interactions are preserved. In addition, we demonstrate that in resting state analyses, APW-MCMV strongly reduces spurious connections while better controlling for false negatives compared to more conservative measures such as symmetrical orthogonalization.

1. Introduction

Since Biswal et al. discovered in 1995 that the sensorimotor cortex activity at rest was correlated with its interhemispheric counterpart, neuroimaging of functional brain connectivity has been the focus of increasing research interest. Brain connectivity has been critical for understanding the intrinsic organization of brain function at rest (Fox et al., 2005; de Pasquale et al., 2010; Yeo and Krienen, 2011; van den Heuvel et al., 2013), as well as how different task demands reshape the organization of large-scale brain connectivity (Krienen et al., 2014; Liljeström and Jan, 2015; Liljeström and Stevenson, 2015; O'Neill et al., 2017; Saarinen et al., 2015; Ribary et al., 2017). Mounting evidence indicates specific functional connectivity alterations in various pathologies of the nervous system (Lynall et al., 2010; Schoonheim et al., 2013; Bozzali et al., 2015; Cerliani et al., 2015; Pang and Snead, 2016; Nunes et al., 2018; Kozhemiako et al., 2019), and adequate methods for studying

interactions among brain regions in function and dysfunction are of critical importance.

Electroencephalography (EEG) and magnetoencephalography (MEG) are modalities very well suited to study brain connectivity dynamics due to their high temporal resolution. To estimate source-space brain dynamics, however, it is necessary to reconstruct the activity at desired brain locations from sensor data located outside the head. We will be using terms “reconstruction” and “estimation” as synonyms further on, although strictly speaking for real data the ground truth is never known and “estimation” is the only option. One popular inverse model method is linearly constrained minimum variance (LCMV) beamforming (Van Veen et al., 1997; Vrba and Robinson, 2001; Sekihara et al., 2002, 2007; Robinson, 2004; Herdman and Douglas, 2009; Moiseev and Herdman, 2013) which has been shown to be very reliable in localizing sources and estimating brain activity (Sekihara et al., 2002; Dalal et al., 2008; Murzin et al., 2011; Jonmohamadi et al., 2014). Inverse modeling, however, is an

* Corresponding author. 2708, 250 - 13450, 102nd Avenue, Surrey, BC V3T 0A3, Canada.

** Corresponding author.

E-mail address: anunessa@sfu.ca (A.S. Nunes).

ill posed problem (Michel et al., 2004; Greenblatt et al., 2005). Its solutions typically exhibit a degree of linear mixing of the estimated brain sources, especially for nearby sources. Connectivity measures sensitive to linear mixing or signal leakage are severely confounded as spurious interactions caused by linear mixing are difficult to distinguish from genuine interactions and this limits the usability and interpretation of the results (Schoffelen et al., 2009).

One way to overcome signal leakage is to use connectivity measures which discard interactions with zero time lags, such as phase lag index (Stam et al., 2007), imaginary coherence (Nolte et al., 2004) and orthogonalized envelope correlations (Brookes et al., 2012; Hipp et al., 2012). However, this is a conservative approach that discards not only signal leakage within the zero phase lag interaction but genuine neurophysiological interactions with small time lags whose existence has been shown to reflect real neural activity by invasive brain recording studies (Brody, 1999; Lachaux et al., 1999; Lutz et al., 2002; Singer, 2010). Also, when time delays do exist, the sensitivity of such connectivity measures may depend on the actual values of the phase difference, the imaginary coherence being a typical example (see Drakesmith et al., 2013 discussing this specific case). Even when magnitudes of the phase lags are formally not involved, such as for Phase Lag Index (PLI), those problems still can't be completely avoided due to inherent discontinuity of any measure designed to be fully sensitive to signals with small time delays and completely insensitive to zero-time delays (see discussion in Vinck and Oostenveld, 2011). Finally, connectivity measures discarding direct zero-lagged interactions are still susceptible to secondary leakage caused by a third source leaking onto the two tested sources at a non-zero phase lag. Although secondary leakage is much smaller, it is still an important confound that renders inaccurate estimates of connectivity (Palva and Matias Palva, 2012; Palva et al., 2018; Wang et al., 2018).

Alternative approaches exist trying to correct for linear mixing without discarding zero-lag interactions. When seed-based connectivity distributions are considered, a straightforward way to deal with direct leakage is to simply subtract the leaked seed signal from the reconstructed target signal (Wens and Marty, 2015). This method works when most of the leakage comes from the seed location but is difficult to generalize to other situations; besides such subtraction results in strong suppression of locations close to the seed region due to limited spatial resolution of the inverse operator. In task-related settings when *connectivity differences* between conditions are investigated, spurious connectivity can be canceled by subtracting connectivity distributions if the conditions have similar power (Liljestrom and Jan, 2015; Liljestrom and Stevenson, 2015). An interesting idea is proposed in a recent work by Ossadtchi and colleagues (Ossadtchi and Altukhov, 2018). First, an inverse problem of reconstructing cross-spectra of the brain sources based on observed cross-spectra of the sensor signals is formulated. Then it is shown that contributions to the sensor cross-spectra arising from spatial spread of forward solutions can be approximately removed by a projection operation in M^2 -dimensional space of all possible pairs of sensor signals, where M is the number of sensors in the array. An exact solution to the projected inverse problem would be a leakage-free reconstruction of all source cross-spectra, at the price of dealing with very high-dimensional "sensor" and "source" spaces (M^2 and n^2 respectively, where n is the number of brain sources). Of course, an approximate inverse solution applied in practice will always exhibit certain degree of leakage due to limited spatial resolution and side lobes of the spatial filter; still this whole idea opens new possibilities that were not explored before.

Multiple Constrained Minimum Variance (MCMV) beamformer, which is used in this study, also deals with linear mixing of reconstructed signals without discarding zero-lagged interactions (Dalal et al., 2006; Popescu et al., 2008; Hui et al., 2010; Moiseev et al., 2011; Quraan & Cheyne, 2010). In this work we will use an approach introduced in Moiseev et al., (2011) for localizing and estimating time courses. This type of MCMV is a multi-source variant of a scalar beamformer (Robinson and Vrba, 1999). We will use the term LCMV to refer to a traditional

single source scalar beamformer. Beamformers work by constructing a spatial filter for a given location that optimally suppresses interference from other locations. MCMV differs from LCMV in that it adds special constraints explicitly preventing linear mixing of reconstructed sources. Specifically, the filter weights for a target location are required to be orthogonal to the forward solutions of all the other sources included in the beamformer (albeit, the number of sources is limited to a few). Consequently, the activity in other locations does not influence the estimation of the activity of a target location, dealing, then, with the signal leakage problem and coherent source cancellation.

In principle such constraints could be added not only to beamformers, as in the cited above papers, but also to other types of inverse solutions (see Hauk and Stenroos, 2014) – for example to minimum norm reconstructions. However, what is often overlooked is that localizer functions used for traditional beamformers, as well as known corrections typically applied to minimum norm solutions to avoid spatial bias (such as dSPM or sLoreta) will no longer work. Thus, in general when a new inverse solution satisfying the "no-leakage" constraints is constructed, new source localizer functions – that is, estimators of source locations and orientations – should also be provided. To our knowledge, no such localizers, for example in Hauk and Stenroos (2014), were described for constrained minimum norm solutions. In contrast, for the MCMV filter discussed here, such localizers were derived in Moiseev et al. (2011); and improved performance of MCMV compared to LCMV was demonstrated (Herdman et al., 2018).

In summary, with MCMV we have a (theoretically) leakage-free spatial filter with known unbiased localizer functions - therefore potentially well suited for connectivity analyses. Its application to such analyses, then, should be investigated in a possibly wider range of practical situations. The aim of this study is to test performance of the MCMV in connectivity analyses, relative to LCMV, under task and rest conditions. An important difference is that in task analyses, a noise covariance can be reliably estimated using inter-trial periods, whereas in resting state analyses those do not exist. This, in addition to poor signal-to-noise ratios, makes resting state connectivity estimates much more difficult and require different approaches, as described below. In the task-related analyses connectivity was estimated using coherence and phase locking values (PLV). First (i), a simple sinusoidal simulation was used to demonstrate spurious connectivity arising from signal leakage and signal cancellation effects. Second (ii), signals from ECoG, similar in complexity as M/EEG signals, were used as ground truth for the simulations. Third (iii), real human MEG recordings of steady-state foveal stimulation task were used to estimate connectivity in entrained areas. For all resting state analyses, envelope correlation was chosen as a connectivity measure due to its demonstrated reliability (Colclough et al., 2016) and popularity in resting state MEG studies. Source reconstruction was done using LCMV, a pair-wise MCMV (PW-MCMV) and an augmented pair-wise MCMV (APW-MCMV). We also used Symmetrical Orthogonalization (SO) applied to the LCMV time series (Colclough et al., 2015), as a reference approach for comparison. Note that this method involves discarding zero-lag interactions. In resting state analyses, first (i) data from a single subject was used to estimate connectivity and construct a simulation where the ground truth was known; second (ii), connectivity in real data was estimated at a group level; and third (iii), surrogate data without genuine connectivity was used to compare group level spurious connectivity (if any) reported by LCMV, MCMV and SO-based methods.

2. Methods

In this manuscript, the following conventions will be used. Scalar quantities and components of matrices and vectors will be denoted by normal lowercase letters, vectors – by bold lowercase letters, and matrices – by bold capital letters. A superscript "T" denotes matrix transposition, and angular brackets (...) denote statistical averaging.

2.1. LCMV spatial filter

In the LCMV approach, the reconstructed brain signal $s_q(t)$ at time t is represented as:

$$s_q(t) = \mathbf{w}_q^T \mathbf{b}(t) \quad (1)$$

here, parameter set $\mathbf{q} = \{\mathbf{r}, \mathbf{u}\}$ consists of source location \mathbf{r} and its orientation \mathbf{u} , the latter being a unit vector; $\mathbf{b}(t)$ is a ($M \times 1$) column vector of sensor readings at time t and M is a total number of sensors in EEG/MEG array; \mathbf{w}_q is a ($M \times 1$) vector of LCMV filter weights. Weight \mathbf{w}_q is selected so that to minimize average reconstructed source power $\langle s_q^2 \rangle$ subject to a unit gain constraint $\mathbf{w}_q^T \mathbf{h}_q = 1$, where \mathbf{h}_q denotes a ($M \times 1$) forward solution vector for the source with parameters. $\mathbf{q} = \{\mathbf{r}, \mathbf{u}\}$.

Assuming that $\mathbf{b}(t)$ is a stationary random process with a zero mean, a well-known result is that optimal filter weights \mathbf{w}_q are given by the expression (Frost, 1972; Van Veen et al., 1997; K. Sekihara et al., 2007):

$$\mathbf{w}_q = \mathbf{R}^{-1} \mathbf{h}_q / (\mathbf{h}_q^T \mathbf{R}^{-1} \mathbf{h}_q) \quad (2)$$

where $\mathbf{R} = \mathbf{b} \mathbf{b}^T$ is the covariance matrix of the sensor data.

2.2. MCMV spatial filter

The MCMV filter generalizes LCMV by reconstructing simultaneously n sources s_{q_i} , $i = 1, \dots, n$. Specifically, a ($n \times 1$) vector of source amplitudes $\mathbf{s} = \{s_{q_1}, \dots, s_{q_n}\}$ is represented as

$$\mathbf{s}(t) = \mathbf{W}^T \mathbf{b}(t) \quad (3)$$

with \mathbf{W} being a ($M \times n$) matrix of weight vectors corresponding to each source: $\mathbf{W} = \{\mathbf{w}_{q_1}, \dots, \mathbf{w}_{q_n}\}$. Weights \mathbf{W} are selected so that to minimize total average reconstructed source power $\sum_{i=1}^n \langle s_{q_i}^2 \rangle = \langle |\mathbf{s}|^2 \rangle$ subject to a constraint $\mathbf{W}^T \mathbf{H} = \mathbf{I}_n$. Here we defined a ($M \times n$) joint forward solution matrix $\mathbf{H} = \{\mathbf{h}_{q_1}, \dots, \mathbf{h}_{q_n}\}$, and \mathbf{I}_n is an n -dimensional identity matrix. The weight matrix which satisfies the minimum variance, i.e. minimum power, is (Frost, 1972; Van Veen et al., 1997; K. Sekihara et al., 2007):

$$\mathbf{W} = \mathbf{R}^{-1} \mathbf{H} (\mathbf{H}^T \mathbf{R}^{-1} \mathbf{H})^{-1} \quad (4)$$

Importantly, due to constraints $\mathbf{W}^T \mathbf{H} = \mathbf{I}_n$, each weight vector \mathbf{w}_{q_i} satisfies a “unit gain condition” with respect to its own forward solution: $\mathbf{w}_{q_i}^T \mathbf{h}_{q_i} = 1$, and a “zero gain” condition with respect to all other sources: $\mathbf{w}_{q_i}^T \mathbf{h}_{q_j} = 0$, $i \neq j$. The latter property makes MCMV beamformer insensitive to source cancellation effects due to source correlations, and prevents linear mixing of reconstructed source time courses.

In MCMV reconstruction, the following approach was used to define the beamformer order. For task-related source estimation, where a limited set of sources of interest could be identified, the order was equal to $n =$ number of sources. For resting state connectivity analysis, we estimated sources using a) a pair-wise MCMV (PW-MCMV) using 2-source MCMV beamformer so that $s_{pair} = \{s_{q_1}, s_{q_2}\}$, thus preventing direct mixing of the sources in the pair, b) an augmented pair-wise MCMV (APW-MCMV) method, detailed below, where in addition to the two sources of interest, we included up to two more sources from locations adjacent to each source of interest, so the maximum beamformer order could reach up to six. The goal was to reduce the possibility of false connectivity in the pair due to *indirect* leakage.

2.3. Source localization

In this section, we give a brief summary of how MCMV and LCMV source localization was performed. Note that when no *a priori* information exists, localization involves finding both source spatial positions and

orientations. In cases when source spatial positions are known, localization procedure only estimates source orientations. Regarding the MCMV approach, details and derivations may be found in Moiseev et al., (2011). LCMV has been used in many studies; a comprehensive analysis and review of relevant literature can be found in (Sekihara and Nagarajan 2008).

In the beamformer method, the sources of brain activity are found using special localizer functions (“localizers”) defined on a source parameter space. The latter includes 3D positions and orientations for each source and therefore has $5n$ dimensions, where n is the beamformer order. The maxima of the localizer points to the true source positions and orientations. It turns out that in both MCMV and LCMV when spatial locations are set, optimal orientations that maximize the localizer can be found up to their sign as solutions of known eigenvalue problems. Thus, orientations can be excluded from the search for the maxima. For this reason, in the expressions below we assume source orientations to be known.

In a general case of oscillatory activity, an unbiased MPZ (that is, multi-source pseudo-Z) localizer is defined as follows:

$$MPZ(q_1, \dots, q_n) = \text{tr}(ST^{-1}) - n \quad (5)$$

where ($n \times n$) matrices S , T are defined as $S = \mathbf{H}^T \mathbf{R}^{-1} \mathbf{H}$ and $T = \mathbf{H}^T \mathbf{R}^{-1} \mathbf{N} \mathbf{R}^{-1} \mathbf{H}$ and N is the ($M \times M$) noise covariance matrix. Note that noise should include all sources of electromagnetic field except the sources of interest targeted by the beamformer. Thus, the noise covariance includes instrumental and environmental noise as well as background brain activity. In the single source LCMV case MPZ is reduced to a well-known expression for pseudo-Z (denoted as Z) up to a constant offset equal to 1:

$$Z(\mathbf{q}) = \frac{\mathbf{w}_q^T \mathbf{R} \mathbf{w}_q}{\mathbf{w}_q^T N \mathbf{w}_q} = \frac{\mathbf{h}_q^T \mathbf{R}^{-1} \mathbf{h}_q}{\mathbf{h}_q^T \mathbf{R}^{-1} \mathbf{N} \mathbf{R}^{-1} \mathbf{h}_q} \quad (6)$$

When dealing with so called evoked activity phase locked to a stimulus, significant increase in SNR and spatial resolution may be achieved by averaging over epochs, which eliminates oscillatory activity as well as noise that are not phase-locked to the stimulus. This leads to event-related (evoked) localizers utilizing epoch-averaged fields. The multi-source evoked response localizer (MER) is defined by expression

$$MER = \text{tr}(ET^{-1}) \quad (7)$$

with ($n \times n$) matrix E defined as $E = \mathbf{H}^T \mathbf{R}^{-1} \bar{\mathbf{C}} \mathbf{R}^{-1} \mathbf{H}$, and $\bar{\mathbf{C}}$ is the second moment of the averaged (“evoked”) field $\langle \mathbf{b} \rangle$; $\bar{\mathbf{C}} = \langle \mathbf{b} \rangle \langle \mathbf{b}^T \rangle$. In a single source case (LCMV) this expression becomes

$$Z_{\text{evoked}}(\mathbf{q}) = \frac{\mathbf{w}_q^T \bar{\mathbf{C}} \mathbf{w}_q}{\mathbf{w}_q^T N \mathbf{w}_q} = \frac{\mathbf{h}_q^T \mathbf{R}^{-1} \bar{\mathbf{C}} \mathbf{R}^{-1} \mathbf{h}_q}{\mathbf{h}_q^T \mathbf{R}^{-1} \mathbf{N} \mathbf{R}^{-1} \mathbf{h}_q} \quad (8)$$

which is analogous to single-source evoked localizers introduced in (Robinson, 2004; Cheyne et al., 2007).

In practice, maxima of the LCMV localizers are easily found by a brute force approach – that is, by calculating localizer values in each and every brain location. In the MCMV case this can’t be done (at least, with a reasonable computational cost) due to high dimensions of the parameter space, and accordingly, approximate iterative procedures are applied (Moiseev et al., 2011; Moiseev and Herdman, 2013; Herdman et al., 2018). Those procedures start with a single-source LCMV beamformer as a first step. In subsequent steps, the beamformer order is incremented, and in the simplest variant already localized sources remain fixed and only the next source is searched by scanning the whole brain volume. In a more complicated and computationally intensive algorithm, the previously found sources are corrected in a secondary iteration loop (Herdman et al., 2018). In this work, the first (simpler) approach was used.

An important requirement for accurate localization is having a good

estimate of the noise covariance N , which participates in all of the expressions (5)–(8) listed above. In task-based studies including the ones presented here, it can be reliably estimated during baseline, stimuli-free intervals, where no task-related activity is present. In resting state studies there is not such an option, and usually diagonal noise (like in this work) or some other substitute for the true noise covariance is used. Locations of interest are also typically defined *a priori* and do not need to be searched for. Still, without a true noise covariance source orientations are determined inaccurately, and might be quite different from the actual ones.

2.4. Augmented pairwise MCMV (APW-MCMV)

In this study, we also introduce “augmented pairwise MCMV” (APW-MCMV) and test its performance relative to LCMV and traditional MCMV for resting state MEG connectivity analysis. In resting state network analyses connectivity is often estimated for all possible pairs of locations of interest (PW-MCMV). A straightforward way to avoid linear mixing, in this case, is to apply 2nd order MCMV beamformer to the target pair. However, this only eliminates direct leakage from one source to another. If either of sources in the pair leaks into a location having strong connection with the other source, *indirect* leakage to a second source will occur, leading to spurious connectivity. Most likely such indirect leakage should happen via areas adjacent to the sources in the pair. This problem can be avoided by including all potential “conductors” of indirect leakage into the beamformer, but this approach has its limitations because besides computational challenges increasing beamformer order adversely affects the SNR of the filter (see Discussion for more details).

Accordingly, we introduce a compromise solution called APW-MCMV, which proceeds as follows. First, connectivity for each pair of sources is estimated using standard pairwise MCMV, and statistically insignificant connections are discarded as described later. Then for every significant pair, we add additional sources to the beamformer based on the following heuristic considerations. Typical spatial resolution of the beamformer in low SNR conditions is around 2 cm. Based on this, we search for neighbors that have significant connections within a 4 cm radius of each of the sources in the pair. If those exist, up to two neighbors of each source in the pair with a maximal total number of connections are included in the beamformer. Including only one such neighbor wouldn't be enough because another neighbor with a comparable strength often exists. Conversely, having three neighbors of comparable strengths is relatively rare; and in any case we do not want the beamformer order to grow too much, as explained in the Discussion section. These considerations result in MCMV order for APW-MCMV calculation being in the range from 2 to 6. This higher order beamformer reconstruction is repeated for every significant pair, and new connectivity estimates are made which are now less likely to be affected by indirect leakage. In Supplemental Materials we show using a single subject resting-state simulation that APW-MCMV performance does not change significantly if the search radius and the number of neighbors are varied within reasonable limits.

2.5. Connectivity measures

For task-related studies, we used coherence and phase locking values to compare the performance of LCMV and MCMV, as metrics sensitive to phase information are most popular in task-based electrophysiological connectivity analyses. To this end, reconstructed brain signals were estimated using beamformer weights derived from broad-band sensor time series. Time-frequency analysis was performed using a multi-taper strategy for decomposing the signal and estimating connectivity in a spectrally-resolved manner (Oostenveld et al., 2011). The multi-taper's frequency-wide smoothing was set to 2 Hz. In the connectivity analyses, we used coherence and phase locking value (PLV) as they capture instantaneous synchrony. Their expressions can be found in Appendix A.

For resting state studies, we compared connectivity from LCMV, PW-

MCMV and APW-MCMV using downsampled envelope correlations, due to their popularity in resting state MEG analyses and due to their previously demonstrated reliability (Colclough et al., 2016). At rest, alpha band oscillators are known to be located in occipital and parietal areas (Goldman et al., 2002), thus resting analyses were carried out in the alpha band as this provides a physiological reference when interpreting connectivity results. Sensor data were band-pass filtered to the 8–12 Hz frequency range. To explore the possibility of using MCMV as an alternative to more conservative methods based on discarding 0-lag connections, we compared the results with the symmetric orthogonalization (SO) technique applied to LCMV reconstructed time courses (Colclough et al., 2015). For the same data, we reconstructed the time courses using LCMV, PW-MCMV and APW-MCMV, and LCMV with SO. In all four cases, amplitude envelope correlations were used to estimate connectivity. The envelopes of the signals were computed by taking the absolute values of the analytic Hilbert transform of the signals and then low-pass filtering to 0.5 Hz.

2.6. Surrogate data

For simulations performed in this study, two types of surrogate data were used. First, we generated *sensor-level* surrogate datasets based on real subjects resting state data, preserving the original data covariance matrix but destroying all true connectivity within this data. This was done by taking time courses of principal components of the covariance matrix, randomizing phases of their Fourier spectra, returning back to the time domain and re-composing a sensor dataset using those “randomized” principal components time courses. Datasets created this way were used in the task-related simulations for construction of the brain noise background, and as a surrogate connectivity-free resting state data.

Second, we generated *source-level* Gaussian surrogate datasets based on reconstructed source time courses of the real resting state data. The goal was to have surrogate source signals with time structure similar to real source signals but having no pairwise connectivity among them. This was done by fitting an autoregressive (AR) model of order one to the reconstructed time courses of real data, then using this model to generate random Gaussian source time courses with the same temporal smoothness. Those were used to establish significance levels for pairwise envelope correlations in resting state analyses.

2.7. Significance testing

To find statistically significant envelope correlations we followed a method suggested in Colclough et al. (2015). Briefly, the correlations were first mapped to $[-\infty, \infty]$ interval using Fisher transformation, then z-scores of the results with zero mean and unit variance were estimated. To calculate the z-scores, we found standard deviations of the transformed correlations of the surrogate connectivity-free data generated using the AR model. The z-scores were then transformed to p-values under Gaussianity assumption, and those were corrected for multiple comparisons using a False Discovery Rate (FDR) threshold equal to 0.05.

2.8. Forward modeling

Point dipole forward solutions were constructed using a single shell head model describing the inner skull boundary (Nolte, 2003). Orientations of all simulated sources (simulations I and II below) were set to be the same and equal to a unit vector $\{1,0,0\}$. Note that with respect to beamformer reconstruction sources with identical orientations are most difficult to resolve, other things being equal. This way the estimates we obtained are likely the most conservative ones. In simulation analyses, the sensor level signal to noise ratio (SNR) was defined as the square root of the ratio of the total average power of all sensors of the pure signal dataset to the total average power of the noise dataset. To estimate effects

of source localization errors on the results we performed reconstructions with both the true lead fields (LFs) and with LFs simultaneously shifted from the correct locations in arbitrary direction by a Gaussian-distributed distances with standard deviations (STDs) of 1, 3 and 5 mm. 500 runs per each STD were done for the task based simulations, and 100 runs for the resting state simulation.

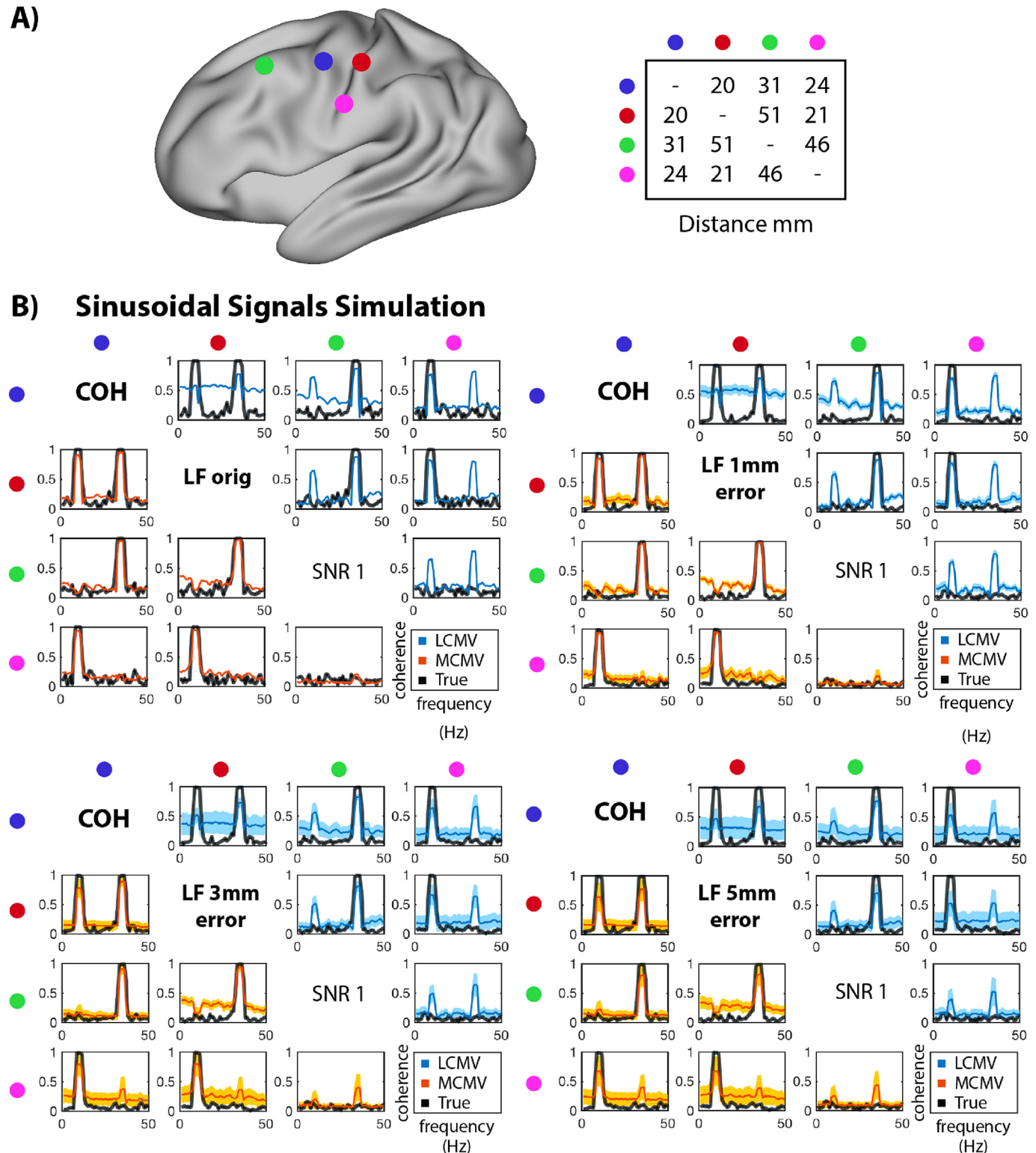


Fig. 1. A) Source locations of the four sources and inter-source distances used in the simulations I and II. B) Coherence between reconstructed sinusoidal signals using LCMV (upper triangle -in blue), MCMV (lower triangle -in red), and the true coherence (in black), with the original LFs and shifted LFs with 1,3 and 5 mm STD scatter. For runs with LF errors coherence averaged over 500 repetitions is plotted, and the shadows represent its standard deviation.

$$s_k = C_k[(1 - \delta_{k3})\sin(2\pi f_1 t) + (1 - \delta_{k4})\sin(2\pi f_2 t) + \epsilon_i], \quad k = 1, \dots, 4 \quad (9)$$

here $f_1 = 10$ Hz, $f_2 = 35$ Hz, t is time in seconds, ϵ is a standard independent Gaussian zero mean random number chosen independently for each time point: $\epsilon_i \sim N(0, 1)$, and δ_{ij} is Kronecker delta. For each k constant C_k was chosen so as to obtain signal RMS equal to 10 nA. Thus, coherence between all sources at 10 Hz was close to 1 except for source 3. Similarly, coherence at 35 Hz for all sources was close to 1 except for source 4. Note that due to zero phase lags between the signals of the same frequency, connectivity between them would simply be ignored by measures insensitive to 0-lag connections. The source signals were projected to the sensors using LFs from the ECoG simulation described below. Surrogate data from a resting state MEG recording was added at the sensor level to model connectivity-free brain noise with an SNR of 2.5. Broad-band covariance (1–50 Hz) was used to calculate beamformer weights using either the original LFs or LFs with 1, 3, and 5 mm error STDs. In all cases source spatial coordinates were assumed to be known *a priori* and set equal to the true ones, while orientations were determined by maximizing corresponding localizers (7) and (8). The aim of this simple simulation was to demonstrate the effects of signal leakage and source cancellation in the LCMV case and compare with the MCMV results for both exact LFs and at different levels of LF errors while keeping the same SNR.

2.9.2. Simulation II: ECoG signals

Electrocorticogram (ECoG) data were used to simulate realistic brain signals, with the same complexity as signals measured with MEG. Data were obtained from an open ECoG database (Miller, 2016), and as requested by the author we reproduce the ethics statement:

The ECoG patient participated in a purely voluntary manner, after providing informed written consent, under experimental protocols approved by the Institutional Review Board of the University of Washington (#12193). The patient data was anonymized according to IRB protocol, in accordance with HIPAA mandate. These data originally appeared in the manuscript “Human Motor Cortical Activity Is Selectively Phase- Entrained on Underlying Rhythms” published in (Miller et al., 2012).

ECoG time series collected from a pre-surgical patient flexing his thumb were used as ground truth. Thumb position was recorded using a 5 degrees of freedom data-glove sensor, thus trials were time locked with the movement onset. Four electrodes with the highest connectivity were selected. The lead fields for voxels closest to the actual electrode position were calculated and data was back projected to the sensors (Fig. 1A). Surrogate sensor data was added at the sensor level to model brain noise, and beamformer weights were calculated using a broad-band covariance (1–50 Hz). Different levels of noise were added to measure the beamformers performance as a function of SNR for different LF errors. Similar to Simulation I, source spatial locations were assumed to be known, while orientations were estimated using LCMV or MCMV localizers.

2.9.3. Real data: steady-state foveal entrainment

MCMV is very well suited for bilateral steady-state brain entrainment in which bilateral sources oscillate at the same phase and frequency producing strong correlations. While MCMV is designed to deal with a few source correlations, LCMV performance is likely to degrade due to the source cancellation effect, and signal leakage should overestimate connectivity in frequencies outside the entrainment.

Data were recorded from four subjects using a 275-channel whole-head MEG system (CTF Systems Inc., Coquitlam, Canada) at a sampling rate of 1200 Hz. The study was approved by the ethics board of Simon Fraser University and all participants consented for the study. The stimulus consisted of a checkerboard circle of 4° alternating black and white at 12 Hz for a period of 3 s, followed by an intertrial interval of 3 s with a fixation cross.

The first stimulus response (FSR) occurs at 6 Hz, half of the

entrainment rhythm, from 0.1 to 0.3 s, and this strong response was used to generate the second moments average matrix \bar{C} for the MER localizer. The signal covariance matrix R was computed from 0.1 to 3 s period, and the noise covariance N from −2.8 to 0 s period. In this case, both spatial locations and orientations of the sources were estimated by performing iterative search over a 5 mm grid and taking first two MER maxima. Then, coherence between the two peaks was estimated between 4 and 45 Hz.

2.10. Resting-state analyses

The data used in the following resting state analyses were obtained from the Human Connectome Project (HCP) and the data were pre-processed as described previously (Larson-Prior et al., 2013). All analyses were performed with 76 sources, with known *a priori* locations, representing each cortical region in the Automatic Anatomical Labeling (AAL, Tzourio-Mazoyer et al., 2002) atlas, and envelope correlation was computed between the source pairs in the alpha band (8–12 Hz). These analysis choices were selected as they reflect popular approaches in the current literature. Sources were reconstructed using an LCMV, a PW-MCMV – two sources reconstructed for each pair-, and an APW-MCMV –where up to four additional sources were included in the beamformer as explained above. In addition, SO was applied to LCMV-reconstructed sources to remove 0-lag interactions. In total, connectivity was estimated with four methods: LCMV, PW-MCMV, APW-MCMV and SO.

2.10.1. Single subject connectivity analysis

Using resting state data collected from a single subject as an example, we compared the four different approaches for estimating functional connectivity using envelope correlations in the real data. Additionally, we performed the same analyses for the simulated data where the ground truth was known. The latter was generated by projecting SO-reconstructed time series back to the sensors and adding surrogate connectivity-free resting state noise background to obtain sensor-level SNR = 2. To estimate effects of LF errors, we ran simulations with 1, 3, and 5 mm error spreads as described above, and calculated averaged Matthew's Correlation Coefficient (MCC), True Positive Rate (TPR) and Positive Prediction Value (see definitions in Appendix A). The higher is the value of each measure – the better is the method's performance. Specifically, higher TPR corresponds to smaller type II errors, higher PPV corresponds to smaller type I errors, and higher MCC reflects a good balance between both type I and II errors (Matthews, 1975), especially when the number of truly existing connections is much smaller than the total number of source pairs.

2.10.2. Group-level connectivity analysis

Connectivity was computed across all the 89 subjects present in the HCP dataset. A fixed effect approach was used to find significant connections and multiple-comparisons corrected using FDR. Then, to assess if the effects found might be driven by signal leakage, the same connectivity analysis was performed using the connectivity-free surrogate data generated using the actual resting state data for the respective subject. Any significant results found in the surrogate analysis would likely indicate spurious connectivity, because even if at the individual level some connections might be significant by chance, at the group level only consistently strong leakage-driven connections would survive.

3. Results

3.1. Task related analyses

3.1.1. Simulation I: sinusoidal signals

In this task-related simulation we contrasted LCMV and MCMV coherence estimates at four locations (Fig. 1A) with the original LFs used

to simulate the sensor data, and with randomly shifted LFs with error spreads of 1, 3 and 5 mm (Fig. 1B). With exact LFs, MCMV is capable of accurately estimating connectivity at coherent frequencies 10 and 35 Hz while suppressing signal leakage everywhere else. LCMV, on the contrary, shows ghost coherence peaks at 10 and 35 Hz between signals coupled at any of these frequencies. In addition, a cancellation effect can be observed at coherent frequencies between coupled signals, where coherence is decreased, and in the first pair, coherence at 10 Hz is at the same level as at other frequencies due to leakage. While real coherence peaks are partially cancelled, ‘ghost peaks’ which are nearly as strong appear.

When localization errors are introduced in the MCMV case, noticeable ‘ghost peaks’ gradually emerge with increasing the error at 35 Hz. The 10 Hz peaks in non-coupled signals are properly nulled, even between source 3 (green) and 2 (red), where the level of coherence noise is elevated.

3.1.2. Simulation II: ECoG signals

We then contrasted performance of LCMV and MCMV for coherence and PLV analyses using more realistic simulated MEG data by using ECoG signals (Fig. 2A) and varied the sensor-level SNR by scaling the added surrogate background brain noise using a) the original LFs; and b) randomized 3 mm STD-shifted LFs. At sensor level SNR = 2.5 and true LFs PLV results are shown in Fig. 2B. The most striking difference between LCMV and MCMV is seen with the motor and sensory source pair (blue and red in Fig. 1A), where LCMV estimates a very high spurious connectivity across the board except for frequencies below 5 Hz, where the estimated connectivity is smaller than the true one. This is caused by source cancellation at low frequencies where the source-level SNR is the highest. Under similar circumstances, PLV estimates tend to be noisier than those for coherence shown in Fig. 2C. This is likely due to the fact that PLV does not take into account instantaneous signal amplitude, thus artificially elevating contributions of small amplitude noise components to the result.

The upper-left panel of Fig. 2C shows coherence estimates obtained using the true LFs at SNR = 2.5. While MCMV performance is almost perfect, LCMV demonstrates strong leakage between pairs where coherence at low frequencies is high. Situation changes radically when random LF shifts with STD = 3 mm are introduced (Fig. 2C, upper right panel): both LCMV and MCMV show practically flat coherence across all source pairs and all frequencies. This happens because at SNR this high source peaks are so narrow that they are simply missed due to the LF errors, and the beamformer effectively samples the noise. With lower SNR = 1 and the same LF error of 3 mm (Fig. 2C, lower left panel) sources are properly picked up and MCMV demonstrates superior performance compared to LCMV. When sensor-level SNR is further decreased (lower right panel of Fig. 2C) MCMV performance deteriorates and for some pairs becomes even worse than that of LCMV (blue-red and blue-green pairs). Specifically, increased pairwise coherence at higher frequencies is observed. The reason for this behavior is that at low SNRs both beamformer maxima and beamformer nulls become wider and can overlap for close by sources. Effectively the beamformer maximum can be canceled by a beamformer null – something that can’t happen for the LCMV filter – resulting in source-level SNRs close to 0. As most of the source power is located in lower frequencies (Fig. 2A), this effect becomes more pronounced at higher frequencies where frequency-specific SNR is smaller – especially minding that filter weights (4) constructed with broad-band covariance are also optimized for lower frequencies carrying the most power. This ramping can be partially or completely eliminated if frequency-specific beamformer weights are constructed, by using covariance matrix R estimated in a narrow frequency band.

3.1.3. Real data: steady-state foveal entrainment

Next, we contrasted the performance of LCMV and MCMV using real MEG data collected during a foveal entrainment paradigm, which was chosen because the relevant neuroanatomy and neurophysiology are

relatively well characterized. Brain entrainment occurs when a stimulus is repetitively presented at a certain frequency. In this study, visual areas representing the fovea were entrained at 12 Hz by presenting a circular grating at about 4–5° in the retina and contrast alternating 6 times per seconds.

In the MCMV source localization employed here (Moiseev et al., 2011), in the first iteration maxima of the MER localizer Eq. (8) coincide with those of LCMV’s evoked pseudo-Z Eq. (9). Importantly, due to source cancellation effect, there is only a single peak corresponding to the strongest source. The other source becomes visible only at the 2nd iteration, when the activity of the 1st source is “nulled” (see brain plots in Fig. 3) and correlated interference is removed.

The first two found MER peaks corresponded to either the foveal representation or the V4 visual area sensitive to motion. Coherence between those was computed using broadband (1–50 Hz) beamformer weights for source reconstruction (Fig. 3 connectivity plots); for LCMV estimates, the 2nd source location found by MCMV was used. As can be clearly seen in Fig. 3, LCMV results generally do not show pronounced isolated peaks at the entrainment frequency or its harmonics. Instead, they often reflect strong source cancellation at 12 Hz (subjects S2, S3). In contrast, MCMV produced a distinct peak at 12 Hz in all cases and also peaks at 24 Hz for subjects S1 and S3. Also, LCMV generally showed increased broad band coherence compared to MCMV which is explained by uncontrolled leakage.

3.2. Resting-state analyses

3.2.1. Single subject connectivity analysis

To compare the performance of LCMV, PW-MCMV and APW-MCMV for resting state MEG connectivity we started with a single subject analysis. First, we estimated connectivity in the actual real data using four methods – namely LCMV, PW-MCMV, APW-MCMV and symmetrically orthogonalized LCMV time courses (SO). Then, we used the time courses obtained by SO to construct a simulated dataset where the ground truth connectivity was known. Specifically, those time courses were projected back to the sensors and connections-free surrogate brain noise data was added at the sensor level. Thus, significant connections discovered in this data which did not exist in the original SO time series must be spurious and would suggest that the same significant connections in the real data were also spurious.

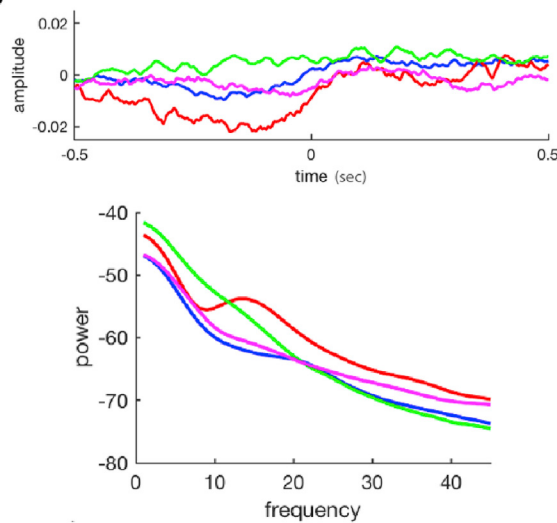
Results for single subject analysis of resting MEG connectivity are presented in Fig. 4A. Alpha band connectivity at rest was expected to be driven in large part by connections involving occipital and parietal areas (Goldman et al., 2002). Clearly, the SO results confirm these expectations. On the contrary, LCMV-based estimates demonstrate strong connections in inferior-frontotemporal and midline areas in addition to parieto-occipital areas. PW-MCMV results are much closer to SO results but still show a few significant connections in inferior-frontotemporal areas. APW-MCMV further corrects the pair-wise approach by discarding most of the connections located anteriorly. With real data it is not possible to be certain if connections are real, or for that matter, if SO results are free from spurious connections.

To identify spurious connections, we simulated data using the SO reconstructed time courses. Thus, the “true” functional connectivity graph was known, and corresponded to the right-most plot in Fig. 4A. The simulation results are depicted in Fig. 4B. Pure LCMV-based connectivity estimates still shows abundant anterior, fronto-temporal and other connections which we can now confidently characterize as spurious. Conversely, the SO approach which seemed the most reliable in the real data turned out to be conservative with numerous true connections being dropped, even though the “true” source time courses were already orthogonalized and therefore should not be discarded by SO. PW-MCMV and especially APW-MCMV results were the ones most close to the ground truth, with APW-MCMV having less spurious connectivity.

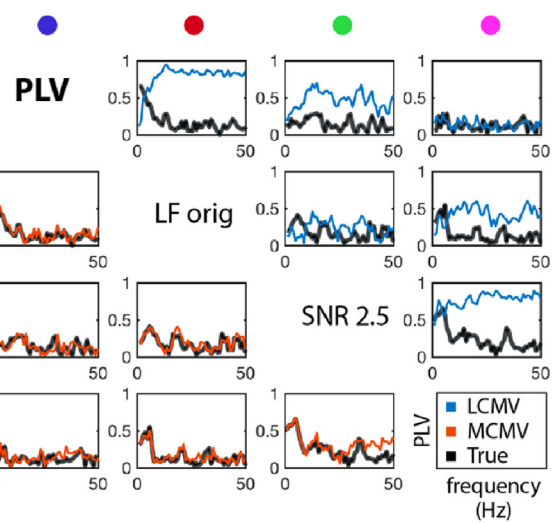
To assess the effect of LF localization errors, we calculated MCC, TPR and PPV for each method with LF shifts STDs set to 1 mm, 3 mm

ECoG Simulation

A)



B)



C)

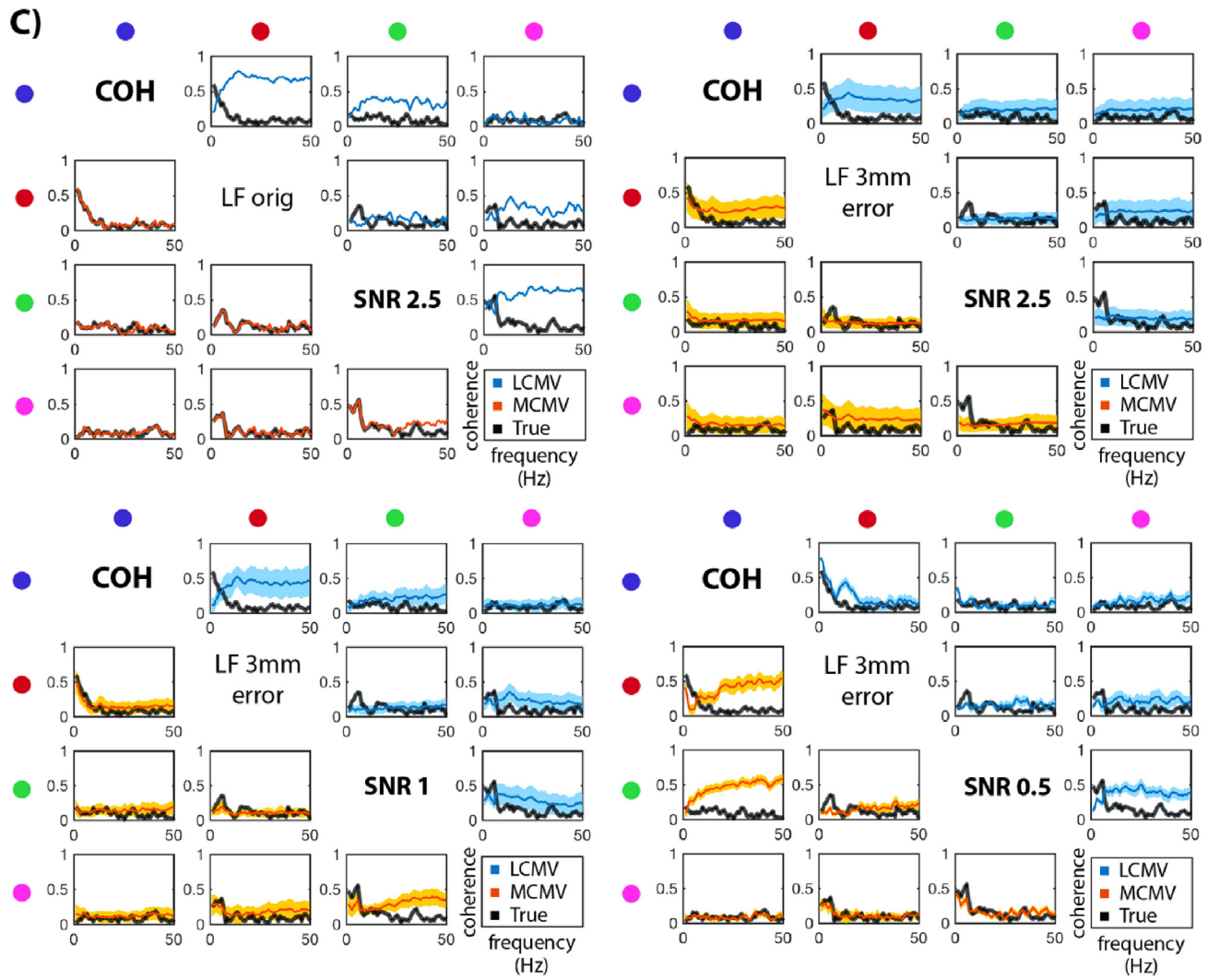


Fig. 2. A) ECoG epoch-averaged time series used in the simulations, and their power spectra. B) PLV connectivity for time courses reconstructed with LCMV (blue), MCMV (red), and the true ones (black) for SNR = 2.5 C) Coherence estimates using the true LFs at SNR = 2.5 and using randomly shifted LFs with STD = 3 mm at SNR = 2.5, 1, and 0.5.

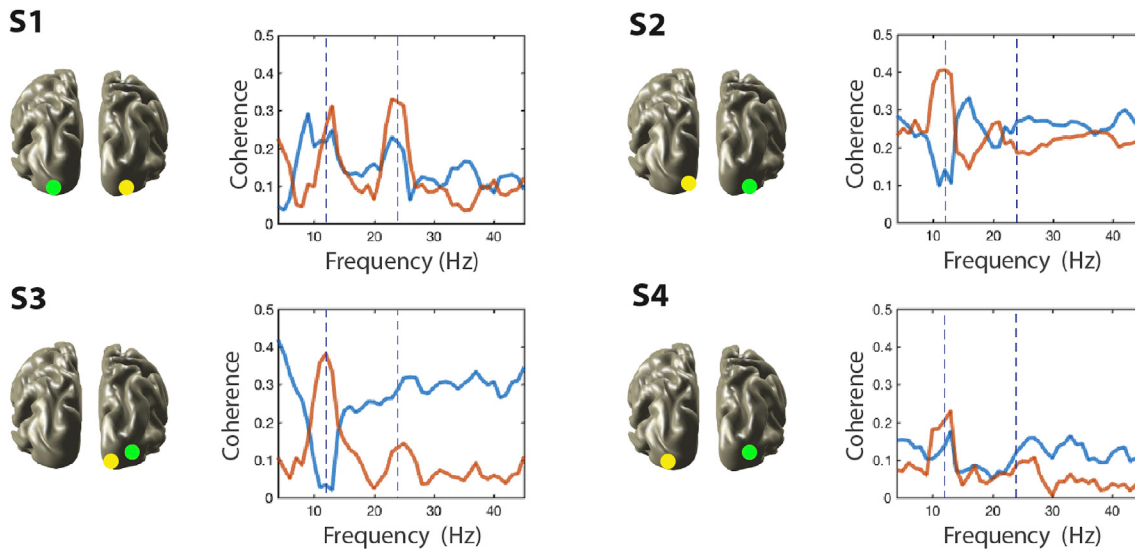


Fig. 3. Visual entrainment of a visual stimuli oscillating at 12 Hz. Four subjects S1 – S4 are presented. Projections of locations of peaks 1 and 2 on the cortex surface are shown with yellow and green circles, respectively. Coherence between the two peaks found was estimated in [4, 45] Hz band using LCMV (blue) and MCMV (orange) reconstructed time courses.

and 5 mm (Fig. 4C). With increased error spread, all four methods slightly degraded. Overall, based on the MCC which is regarded as the most suitable statistical measure for such cases, APW-MCMV provides the best trade-off between type I and type II statistical errors. SO, on the other side, provides much more control of false positives (type I error) at the expense of discarding true positives (type II error). It should also be noted that while advantage of APW-MCMV compared to simple PW-MCMV in terms of MCC becomes insignificant for larger LF errors, APW-MCMV still provides better control over the false positives, as the PPV plot shows.

3.2.2. Group-level connectivity analysis

To further contrast the performance of LCMV, PW-MCMV, APW-MCMV and SO for resting MEG connectivity, analyses described in the previous section were applied to each of the 89 subjects in the HCP dataset, then results were further corrected for multiple comparisons at 0.05 FDR level (Fig. 5). In general, group-level results follow the pattern observed in the single subject case, with LCMV demonstrating lots of potentially spurious connections and SO being the most conservative.

3.2.3. Surrogate data group-level analysis

To contrast the susceptibility of each of the compared methods to spurious connectivity, we performed a connectivity analysis of ‘null’ (surrogate) data. Compared to the single subject case above, however, these seemingly spurious connections in the group level could be real as the ground truth is unknown. To reveal connections that are guaranteed to be false we performed the same group level connectivity analysis with each subject’s data replaced with corresponding connectivity-free surrogate sensor data. After that, no significant connections should have been found at a group level. This was indeed the case with SO, while with LCMV a great number of connections were found significant in inferior frontotemporal and midline areas as in the previous single subject analysis. In the MCMV cases the number of “significant” spurious connections were very small, particularly with APW-MCMV with only 3 false positives (Fig. 6A). Still, it can be noted that while SO spatial connectivity lacked any discernible pattern (Fig. 6B), for MCMVs connectivity matrices there is a clear spatial pattern. This pattern is very pronounced in LCMV, giving rise to many false positives. The pattern increasingly improves and fades out with PW- and APW-MCMV, albeit do not completely disappear.

4. Discussion

In this study, we demonstrate the advantages of using MCMV method when estimating functional connectivity in the brain based on beamformer source reconstruction. We show using real and simulated data that MCMV outperforms LCMV by better suppressing signal leakage and coherence signal cancellation in task conditions using inter-regional phase synchronization and coherence analysis, and in resting state for mapping inter-regional amplitude correlations. In addition, for resting state analyses we introduce an APW-MCMV approach which further reduces spurious connectivity compared to PW-MCMV.

To a large degree, MCMV prevents signal leakage, which is the main cause of spurious connectivity found by a traditional LCMV beamformer. Importantly, MCMV does not “correct” an existing inverse solution for leakage; instead it provides a (ideally) leakage-free solution from the very beginning, by making source weights orthogonal to forward solutions of the interfering sources. A variety of alternative methods start with traditional inverse solutions instead, and then try to eliminate signal leakage by discarding 0-lag connections. Among those methods we chose symmetrical orthogonalization approach described in Colclough et al. (2015) for comparisons, since it shows a good performance and provides a strong control for false connections. Note that SO has much in common with other methods based on the source time courses orthogonalization (Brookes et al., 2012; Brookes et al., 2014; Hipp et al., 2012), which makes us believe that our results relate to those also. To avoid confusion, we would like to point out that source time courses orthogonality and weights/forward solution orthogonality imposed by MCMV have completely different physical meaning. In particular, the latter does not penalize 0-lag connections. Especially for the resting state scenarios, we wanted to investigate if MCMV could deliver similar performance but without limitations imposed by SO and related techniques. In particular, we wanted to be able to address situations when connections with short propagation times are important and should not be discarded, or when one needs to look at finer time scales than amplitude time courses would allow, so that other connectivity measures, such as PLV or coherence, should be applied.

As a technical note, it should be mentioned that if we limit ourselves to connectivity measures based on the 2nd moments of the source cross-spectra, explicit source time course construction can be avoided by creating MCMV spatial filter in the frequency domain. Corresponding expressions only involve the observed sensor-level cross-spectra and

forward solutions of participating locations. Such an approach could be called a multi-source generalization of the DICS method (Gross et al., 2001), and could be used, for example, to plot seed-based coherence or PLV spatial distributions. However, one still needs to reconstruct source time courses explicitly when other connectivity measures (specifically – envelope correlations) are involved, like in this work.

In this work we demonstrated that in both task and resting state scenarios MCMV outperformed LCMV by greatly reducing, albeit not completely discarding, spurious connectivity, despite the fact that 0-lag connections were included. For the resting-state functional connectivity, our *augmented pairwise-MCMV* approach was shown to further reduce spurious connections compared to simple *pairwise-MCMV*. We focused on

Single subject connectivity

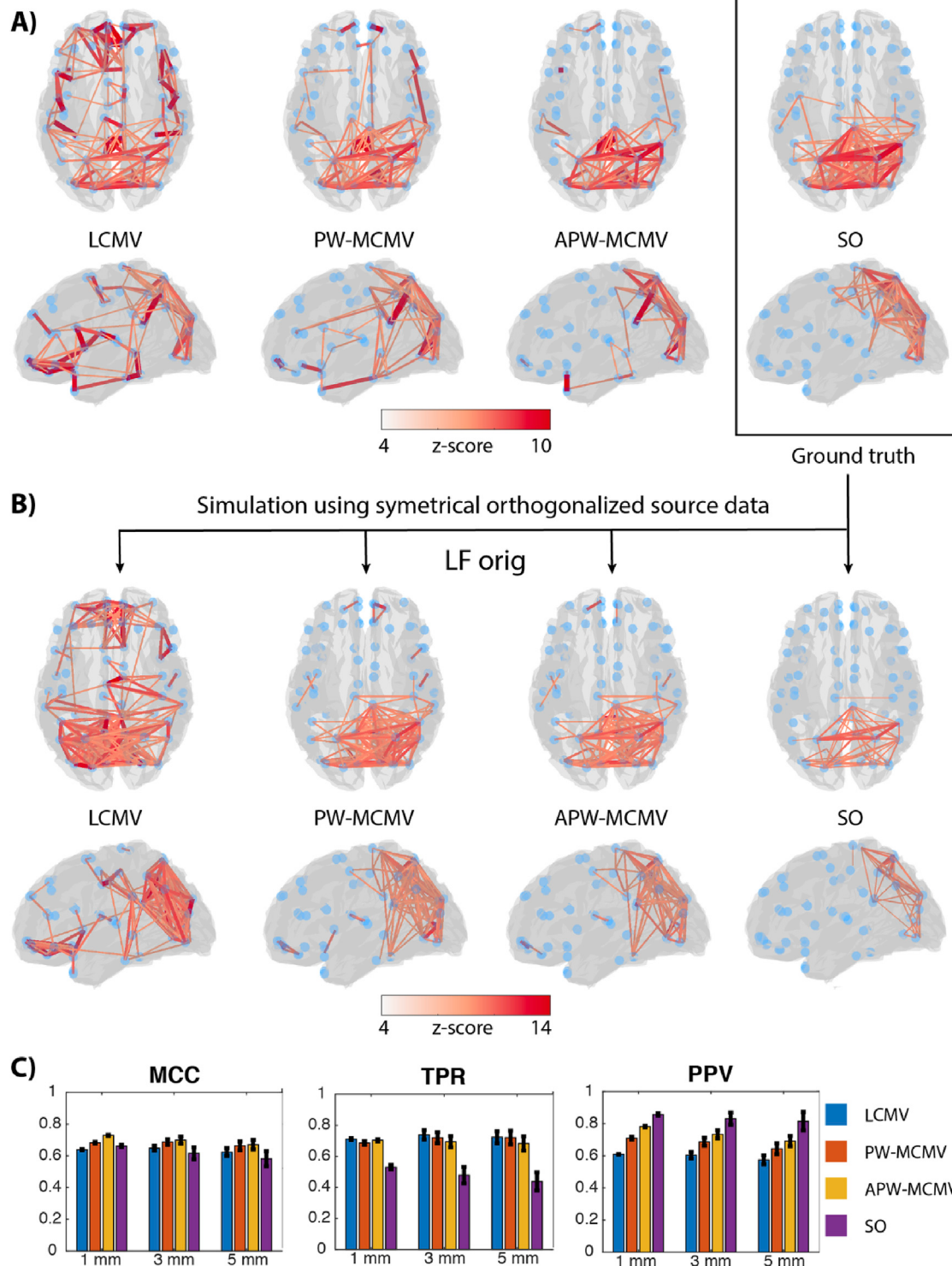


Fig. 4. Single subject resting state connectivity analysis. A) Significant alpha-band amplitude envelope correlations in the real data obtained with LCMV, PW-MCMV, APW-MCMV and SO. B) Same analyses applied to the simulated resting state data with the “ground truth” connectivity corresponding to the right-most panel of (A). C) MCC, TPR and PPV for LF error STDs = 1, 3 and 5 mm averaged over 100 simulation runs; the error bars correspond to ± 1 standard deviation of the results.

Group level connectivity

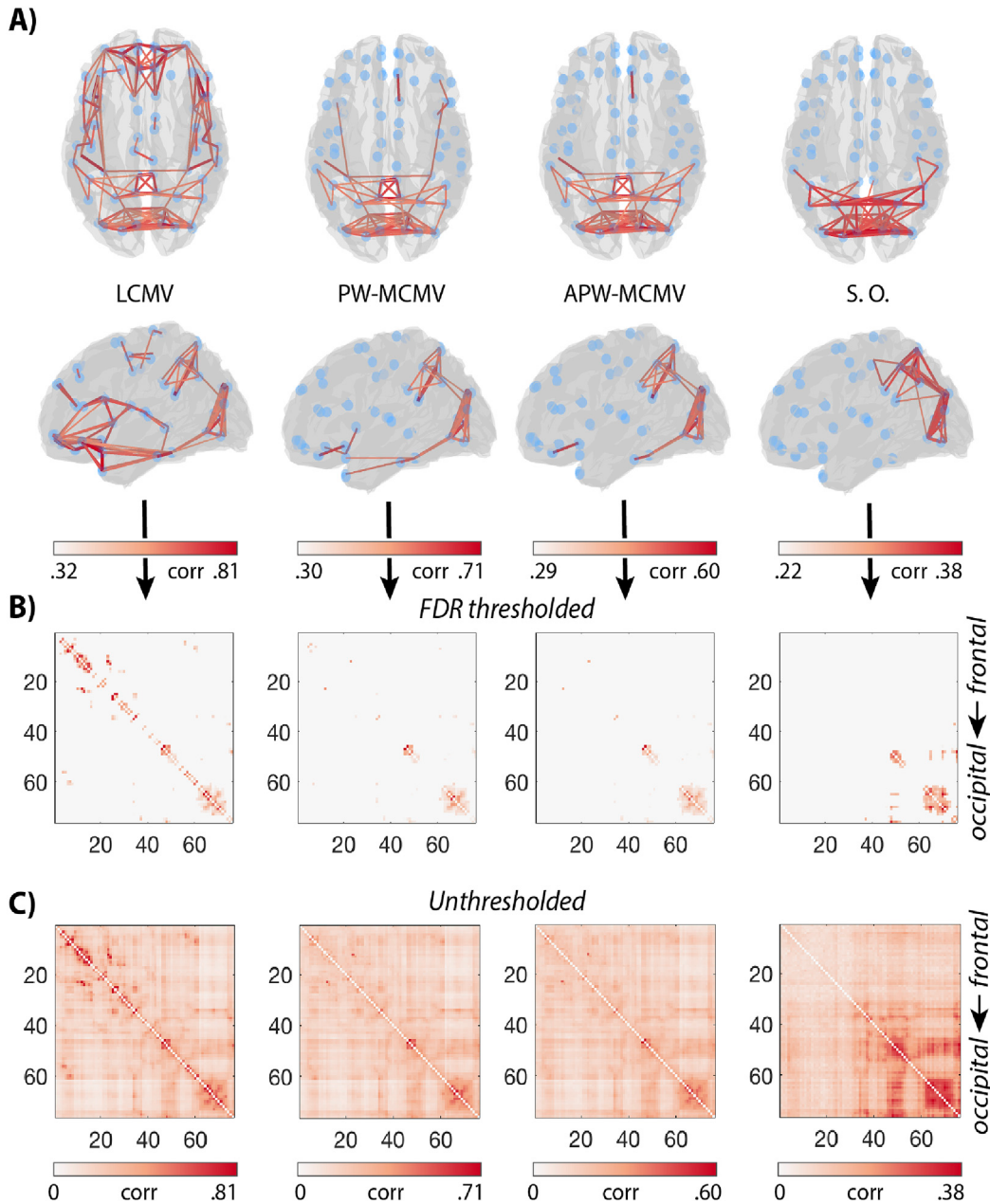


Fig. 5. Group-level envelope correlation analysis. A) Significant connections FDR corrected plotted in brain space. B) Connectivity matrices thresholded with only significant connections. C) Raw connectivity matrices depicting the spatial connectivity pattern. For visualization purposes, the correlation values were used instead of the z-scores. Connections closer to the diagonal represent spatially closer source pairs.

connectivity analyses of task-related activity and resting state activity, which are the two most common scenarios encountered in basic and clinical research. There are differences in how beamformers are applied in each case. When there are few sources of activity, but their spatial locations are not known in advance, beamformer reconstruction involves searching the brain for active sources. Task-related scenarios often (but not always) fall into this category. Importantly, in task related measurements noise covariance can be properly estimated using control intervals, and higher SNRs are achievable via trial averaging. By applying MCMV localizers (Moiseev et al., 2011), it becomes possible to accurately find source positions and orientations even for highly correlated sources. An alternative situation to consider is when source locations are known or selected *a priori*, however the number of sources n is large and SNR is close to zero; resting state analyses are a typical example. In this case one

can't use beamformer orders equal to n because n is too large, as discussed in more detail below. In addition, particularly in the resting state case there are no such "control" intervals where we know for sure that selected sources are silent. As a result, there is no way to measure the noise covariance with respect to those sources. As source orientations still need to be found from the data, this is done by plugging into MCMV localizers (5) or (6) "ad hoc" noise covariance (i.e. a diagonal one), resulting in inaccurately estimated source orientations. All these factors result in poorer source reconstruction and less reliable connectivity estimates.

The MCMV has known weaknesses, complicated source search procedures being one of them (Moiseev et al., 2011; Moiseev and Herdman, 2013; Herdman et al., 2018). Another weakness of MCMV is dependence of the SNR of the beamformer on its order and on relative locations of the

Group level null connectivity

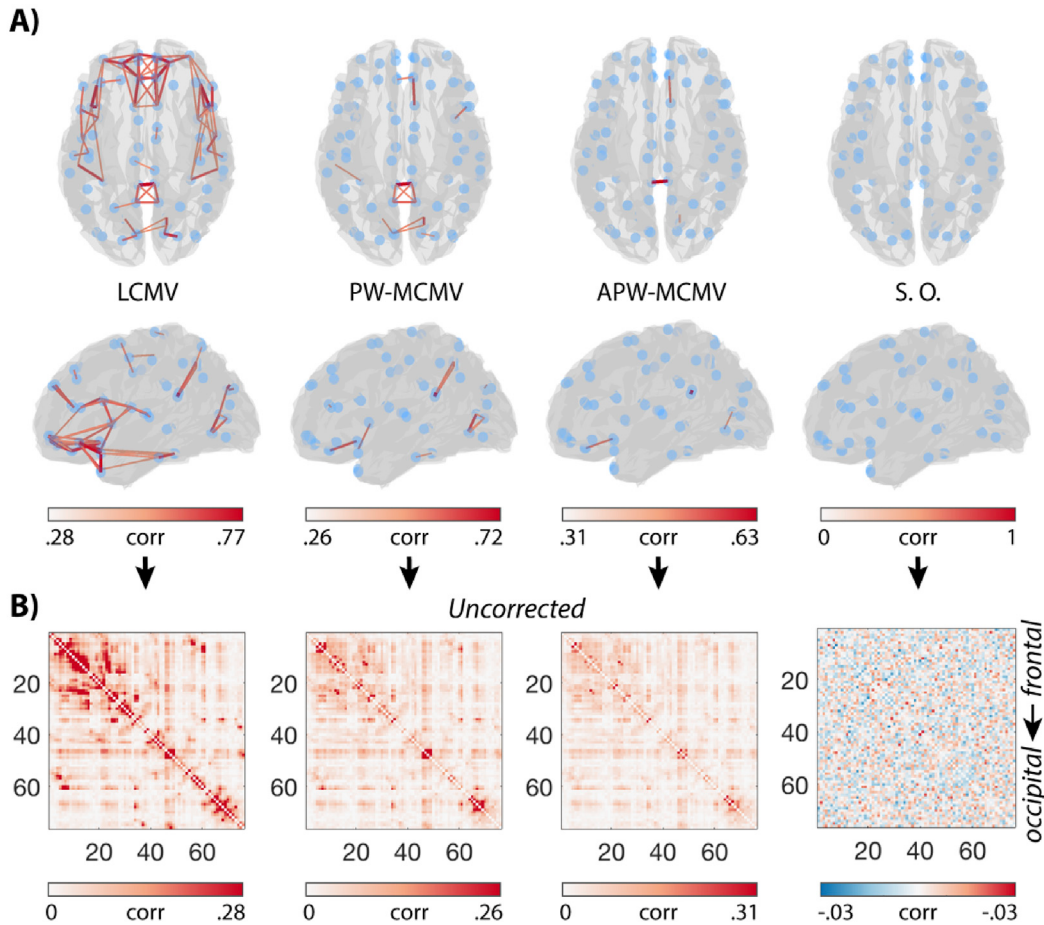


Fig. 6. Connectivity for each subject estimated using surrogate sensor data. A) Significant connections at the group level. B) Correlation matrices. Upper limits of the color scales correspond to the statistical significance thresholds. Connections closer to the diagonal represent less spatially separated source pairs.

sources, as discussed below. In particular, in resting state analyses this prevents from using beamformer orders close to the rank of the data in order to have mutual leakage correction simultaneously between all the sources similarly to the SO method. A general reason why an increase beamformer order leads to decrease in SNR is because for n -source beamformer only $M - n$ degrees of freedom are left for interference suppression. This can be imagined as losing n sensors of the array. At first glance, this should not significantly affect the SNR if $n \ll M$, which for modern MEG systems should allow dealing with many (say, 40–50) sources simultaneously. It turns out though that the limitation is much more severe when the relative positions of the sources are considered. For example, sources residing in the same lobe will be mostly seen by a smaller number of M_{actual} sensors located closer to that lobe, $M_{actual} \ll M$. Effective limiting condition in such case will be $n/M_{actual} \ll 1$ which becomes violated at much smaller n . This is why in practice one would not want to use beamformer orders more than 8 or 10 (See also Fig. B1 in Supplemental materials).

Additionally, due to finite spatial resolution, the nulls imposed by the MCMV beamformer are not points but rather areas of certain size in the signal space. In the worst case situations when sources are sufficiently close to each other, the nulls imposed on neighboring sources overlap with the target source, making the SNR extremely poor and MCMV weights very “fine-tuned” to the interference. ECoG simulation provides an example of how it happens in practice. Here we did not see problems while the sensor-level SNR was high. In low SNR cases, when the filter weights were constructed using the broadband covariance, the beamformer still continued to perform well for lower frequencies, where most

of the signal and noise power were concentrated. However, for pairs involving closer sources (blue and red, blue and green in Fig. 2C) these weights turned out to be no longer optimal at higher frequencies, resulting in MCMV reporting spurious connectivity there (see Fig. 2C). If frequency-specific narrow band covariance is used for weights construction, this spurious connectivity disappears. Accordingly, using a narrow-band covariance (that is, “tuning” the weights depending on the frequency) whenever possible seems advantageous because in practice neither signals nor noise have flat power spectra. It is also interesting to point out how LCMV filter inverted the true signal coherence (Fig. 2B and C) yielding completely distorted frequency dependence. In this case, source cancellation played a major role. The cancellation was most pronounced at the low end of the spectrum where both the true coupling and the SNR were high, or at strong coherent 10 or 35 Hz peaks in the sinusoidal simulation. As a result, reported coherence was minimal. At higher frequencies, the source signals canceled less, and estimated coherence grew due to strong uncontrolled leakage.

The human steady-state foveal entrainment MEG study provided a good example of a situation where LCMV approach fails due to both signal leakage and source cancellation occurring for strongly correlated activity. At the same time, methods of leakage correction that discard the instantaneous interaction between two signals would be obviously unsuitable here. In this experiment, MCMV revealed connectivity in areas associated with foveal representation, whereas LCMV connectivity was smeared across the visual cortices. Based on this, we believe that future studies could benefit from using MCMV to estimate highly synchronous activity occurring when separate brain areas are simultaneously paced by

the same stimulus.

In our resting-state analyses, we compared connectivity estimates obtained with LCMV, MCMVs and SO approaches at a single-subject and group levels, for real and surrogate data. We used the SO approach as a conservative reference method with a strong control for spurious connectivity due to signal mixing at the expense of discarding zero-lag connections.

In the single-subject case, we found that LCMV greatly overestimates connectivity in inferior frontotemporal and midline areas. In contrast, with orthogonalized signals the only significant connections were located in posterior-parietal and occipital areas, where alpha generators are expected (Goldman et al., 2002). Pairwise (two-source) MCMV mostly eliminated spurious couplings reported by LCMV, however, it still reported more connections than SO. The APW-MCMV results were close to those observed for SO. The simulation where the ground truth connectivity was known, showed that even at relatively high SNR = 2, the SO method was conservative discarding true connections but keeping only true ones, while MCMV-based approaches preserved those, at the expense of showing more false positives. This effect was still present when introducing random LF shifts from true locations with STDs equal to 1, 3 and 5 mm. This illustrates a well-known tradeoff between type I and type II statistical errors which is quantified in Fig. 4C, where SO is showing the best PPV rates, as expected, but is not overall optimal, as MCC results suggest. It is worth noting though that in practical situations controlling for type II error (false negatives) is as important as controlling for false positives, or even may be a priority. The MCMV-based approaches seem to suggest more balance between the two errors and have an additional advantage of taking 0-lag connections into account.

The group level analyses confirmed the results found in the single-subject case. When the group analysis was performed with the subjects' connectivity-free surrogate data, we found that the connectivity

matrix for SO did not display any spatial pattern, as should be expected. LCMV and MCMVs had a clear spatial pattern, however, while in LCMV this pattern was strong enough to produce lots of false connections appearing as being significant, with PW-MCMV only a few such connections remained, and with APW-MCMV those were almost eliminated.

5. Conclusion

In this comprehensive study, we investigated the advantages of MCMV spatial filters for analyses of noninvasive electrophysiological functional connectivity in the human brain. Using simulated and real data in task-related and resting state scenarios, we demonstrated how MCMV-based approaches address the problem of spurious connectivity arising from signal mixing and coherent source cancellation, without discarding connections with very short or zero-time delays. We also showed that MCMV, while strongly reducing spurious connections obtained with traditional LCMV reconstruction, provides better control over type II statistical error than more conservative methods based on completely discarding 0-lag interactions between the signals.

Data and code availability statement

Data used in this manuscript is mostly based on open access repositories, and code has been previously published in Moiseev et al., (2011). Both are available on request.

Acknowledgements

This study was supported by the Canadian Institutes of Health Research (www.cihr-irsc.gc.ca) CIHR grant to S. M. D. (MOP-136935) and NSERC grant to S. M. D. (RGPIN-435659).

Appendix A

Connectivity measures

PLV is a measure of phase synchrony between two signals calculated by averaging the phase difference θ between complex-valued narrow-band time series (Lachaux et al., 1999). For a pair of such signals x and y PLV is estimated according to the expression:

$$PLV_{x,y} = \left| \left(\sum_{k=1}^N e^{i\theta_k} / N \right) \right|$$

here N is the number of epochs, and θ_k is the phase difference between the signals in k -th epoch.

The coherence between two signals x and y is defined via their power spectra and cross spectra at specific frequency f by the formula:

$$Coh_{xy}(f) = \frac{|S_{xy}(f)|^2}{S_{xx}(f) \cdot S_{yy}(f)}$$

where S_{xy} denotes the cross spectrum of the signals at frequency f .

Definitions of binary classifier performance indices as applied to connectivity analyses

Let N_{pairs} be the total number of possible pairwise connections. Assume that in reality there are only p connected pairs ("true connections"), so the following always holds: $N_{pairs} = p + n$, where n is the number of false (non-existing) connections. As for any binary classifier, a connectivity estimation result can be characterized by: *true positives* (tp) – the number of actually existing connections among all significant connections found; *false positives* (fp) – the number of connections found significant but non-existing in reality; *true negatives* (tn) – the number of actually disconnected pairs among all found disconnected pairs; *false negatives* (fn) – the number of true connections labeled as non-existent. Based on these, the following performance characteristics are defined:

True Positive Rate (TPR), or sensitivity: $TPR = tp/p$;

Positive Prediction Value (PPV), or precision: $PPV = tp / (tp + fp)$;

$$\text{Matthews Correlation Coefficient (MCC): } MCC = \frac{tp \cdot tn - fp \cdot fn}{\sqrt{(tp + fp)(tp + fn)(tn + fp)(tn + fn)}}.$$

Appendix B. Supplementary data

Supplementary data to this article can be found online at <https://doi.org/10.1016/j.neuroimage.2019.116386>.

References

- Bozzali, Marco, Dowling, Claire, et al., 2015. "The impact of cognitive reserve on brain functional connectivity in Alzheimer's disease. *J. Alzheimer's Dis.* 44 (1), 243–250.
- Brody, Carlos D., 1999. Disambiguating different covariation types. *Neural Comput.* 11 (7), 1527–1535.
- Brookes, M.J., Woolrich, M.W., et al., 2012. Measuring functional connectivity in MEG: a multivariate approach insensitive to linear source leakage. *Neuroimage* 63 (2), 910–920.
- Brookes, Matthew J., Woolrich, Mark W., et al., 2014. An introduction to MEG connectivity measurements. In: *Magnetoencephalography: from Signals to Dynamic Cortical Networks*.
- Cerliani, Leonardo, Mennes, Maarten, et al., 2015. Increased functional connectivity between subcortical and cortical resting-state networks in autism spectrum disorder. *JAMA Psychiatry* 72 (8), 767–777.
- Cheyne, Douglas, Bostan, Andreea C., et al., 2007. Event-related beamforming: a robust method for presurgical functional mapping using MEG. *Clin. Neurophysiol.* 118 (8), 1691–1704.
- Colclough, G.L., Brookes, M.J., et al., 2015. A symmetric multivariate leakage correction for MEG connectomes. *Neuroimage* 117, 439–448.
- Colclough, G.L., Woolrich, M.W., et al., 2016. How reliable are MEG resting-state connectivity metrics? *Neuroimage* 138, 284–293.
- Dalal, Sarang S., Guggisberg, Adrian G., et al., 2008. Five-dimensional neuroimaging: localization of the time-frequency dynamics of cortical activity. *Neuroimage* 40 (4), 1686–1700.
- Dalal, Sarang S., Sekihara, Kensuke, et al., 2006. Modified beamformers for coherent source region suppression. *IEEE (Inst. Electr. Electron. Eng.) Trans. Biomed. Eng.* 53 (7), 1357–1363.
- Drakesmith, M., El-Deredy, W., Welbourne, S., 2013. Reconstructing coherent networks from electroencephalography and magnetoencephalography with reduced contamination from volume conduction or magnetic field spread. *PloS one* 8 (12), e81553.
- Fox, Michael D., Snyder, Abraham Z., et al., 2005. The human brain is intrinsically organized into dynamic, anticorrelated functional networks. Source: *Proc. Natl. Acad. Sci. U. S. A* 102 (27), 9673–9678.
- Frost, O.L., 1972. An algorithm for linearly constrained adaptive array processing. *Proc. IEEE* 60 (8), 926–935.
- Goldman, Robin I., Stern, John M., et al., 2002. Simultaneous EEG and fMRI of the alpha rhythm. *Neuroreport* 13 (18), 2487–2492.
- Greenblatt, Richard E., Ossadtchi, Alexei, et al., 2005. Local linear estimators for the bioelectromagnetic inverse problem. *IEEE Trans. Signal Process.* 53 (9), 3403–3412.
- Gross, J., Kujala, J., et al., 2001. Dynamic imaging of coherent sources: studying neural interactions in the human brain. *Proc. Natl. Acad. Sci. U. S. A* 98 (2), 694–699.
- Hauk, Olaf, Stenroos, Matti, 2014. A framework for the design of flexible cross-talk functions for spatial filtering of EEG/MEG data: DeFleCT. *Hum. Brain Mapp.* 35 (4), 1642–1653.
- Herdman, Anthony T., Douglas, Cheyne, 2009. A practical guide for MEG and beamforming. In: *Brain Signal Analysis: Advances in Neuroelectric and Neuromagnetic Methods*, pp. 1–36.
- Herdman, Anthony T., Moiseev, Alexander, et al., 2018. Localizing event-related potentials using multi-source minimum variance beamformers: a validation study. *Brain Topogr.* 31 (4), 546–565.
- Tzourio-Mazoyer, N., Landeau, B., Papathanassiou, D., Crivello, F., Etard, O., Delcroix, N., Mazoyer, B., Joliot, M., 2002. Automated Anatomical Labeling of Activations in SPM Using a Macroscopic Anatomical Parcellation of the MNI MRI Single-Subject Brain. *Neuroimage* 15, 273–289.
- van den Heuvel, Martijn, P., Sporns, Olaf, 2013. Network hubs in the human brain. *Trends Cogn. Sci.* 17 (12), 683–696.
- Hipp, Joerg F., Hawellek, David J., et al., 2012. Large-scale cortical correlation structure of spontaneous oscillatory activity. *Nat. Neurosci.* 15 (6), 884–890.
- Hui, Hua Brian, Pantazis, Dimitrios, et al., 2010. Identifying true cortical interactions in MEG using the nulling beamformer. *Neuroimage* 49 (4), 3161–3174.
- Jommohamadi, Yaqub, Poudel, Govinda, et al., 2014. Comparison of beamformers for EEG source signal reconstruction. *Biomed. Signal Process. Control* 14 (1), 175–188.
- Kozhemiako, N., Nunes, A., Vakorin, V.A., Chau, C.M., Moiseev, A., Ribary, U., Doesburg, S.M., 2019. Atypical resting state neuromagnetic connectivity and spectral power in very preterm children. *J. Child Psychol. Psychiatry*.
- Krienen, F.M., Yeo, B.T.T., et al., 2014. Reconfigurable task-dependent functional coupling modes cluster around a core functional architecture. *Philos. Trans. R. Soc. Biol. Sci.* 369 (1653), 20130526–20130526.
- Lachaux, Jean Philippe, Rodriguez, Eugenio, et al., 1999. Measuring phase synchrony in brain signals. *Hum. Brain Mapp.* 8 (4), 194–208.
- Larson-Prior, L.J., Oostenveld, R., et al., 2013. Adding dynamics to the human connectome Project with MEG. *Neuroimage* 80, 190–201.
- Liljeström, M., Jan, K., et al., 2015a. Dynamic reconfiguration of the language network preceding onset of speech in picture naming. *Hum. Brain Mapp.* 36(3), -36 (3), 1202–1216.
- Liljeström, Mia, Stevenson, Claire, et al., 2015b. Task- and stimulus-related cortical networks in language production: exploring similarity of MEG- and fMRI-derived functional connectivity. *Neuroimage* 120, 75–87.
- Lutz, A., Lachaux, J.P., et al., 2002. Guiding the study of brain dynamics by using first-person data: synchrony patterns correlate with ongoing conscious states during a simple visual task. *Proc. Natl. Acad. Sci.* 99 (3), 1586–1591.
- Lynall, M.E., Bassett, D.S., et al., 2010. Functional connectivity and brain networks in schizophrenia. *J. Neurosci.* 30 (28), 9477–9487.
- Matthews, B.W., 1975. Comparison of the predicted and observed secondary structure of T4 phage lysozyme. *Biochim. Biophys. Acta Protein Struct.* 405 (2), 442–451.
- Michel, Christoph M., Murray, Micah M., et al., 2004. EEG source imaging. *Clin. Neurophysiol.* 115 (10), 2195–2222.
- Miller, K.J., 2016. A Library of Human Electrocorticographic Data and Analyses. Stanford Digital Repository. Available at: <https://purl.stanford.edu/zk881ps0522>.
- Miller, Kai J., Hermes, Dora, et al., 2012. Human motor cortical activity is selectively phase-entrained on underlying rhythms. *PLoS Comput. Biol.* 8 (9), e1002655 edited by T. Behrens.
- Moiseev, Alexander, Gaspar, John M., et al., 2011. Application of multi-source minimum variance beamformers for reconstruction of correlated neural activity. *Neuroimage* 58 (2), 481–496.
- Moiseev, Alexander, Herdman, Anthony T., 2013. Multi-core beamformers: derivation, limitations and improvements. *Neuroimage* 71, 135–146.
- Murzin, Vyacheslav, Fuchs, Armin, et al., 2011. Anatomically constrained minimum variance beamforming applied to EEG. *Exp. Brain Res.* 214 (4), 515–528.
- Nolte, Guido, 2003. The magnetic lead field theorem in the quasi-static approximation and its use for magnetoencephalography forward calculation in realistic volume conductors. *Phys. Med. Biol.* 48 (22), 3637–3652.
- Nolte, Guido, Ou, Bai, et al., 2004. Identifying true brain interaction from EEG data using the imaginary part of coherency. *Clin. Neurophysiol.* 115 (10), 2292–2307.
- Nunes, A.S., Peatfield, N., Vakorin, V., Doesburg, S.M., 2018. Idiosyncratic organization of cortical networks in autism spectrum disorder. *Neuroimage*.
- O'Neill, George C., Tewarie, Prejaas K., et al., 2017. Measurement of dynamic task related functional networks using MEG. *Neuroimage* 146, 667–678.
- Oostenveld, Robert, Pascal, Fries, et al., 2011. FieldTrip: open source software for advanced analysis of MEG, EEG, and invasive electrophysiological data. *Comput. Intell. Neurosci.* 2011.
- Palva, J. Matias, Puoliväli, Tuomas, et al., 2018. Hyperedge bundling: a practical solution to spurious interactions in MEG/EEG source connectivity analyses. *Neuroimage* 173, 610–622.
- Ossadtchi, A., Altukhov, D., et al., 2018. Phase shift invariant imaging of coherent sources (PSIICOS) from MEG data. *Neuroimage* 183, 950–971.
- Palva, Satu, Matias Palva, J., 2012. Discovering oscillatory interaction networks with M/EEG: challenges and breakthroughs. *Trends Cogn. Sci.* 16 (4), 219–229.
- Pang, Elizabeth W., Snead III, O.C., 2016. From structure to circuits: the contribution of MEG connectivity studies to functional neurosurgery. *Front. Neuroanat.* 10, 67.
- de Pasquale, F., Della Penna, S., et al., 2010. Temporal dynamics of spontaneous MEG activity in brain networks. *Proc. Natl. Acad. Sci.* 107 (13), 6040–6045.
- Popescu, Mihai, Popescu, Elena Andra, et al., 2008. Spatio-temporal reconstruction of bilateral auditory steady-state responses using MEG beamformers. *IEEE (Inst. Electr. Electron. Eng.) Trans. Biomed. Eng.* 55 (3), 1092–1102.
- Quraan, Maher A., Cheyne, Douglas, 2010. Reconstruction of correlated brain activity with adaptive spatial filters in MEG. *Neuroimage* 49 (3), 2387–2400.
- Ribary, U., Doesburg, S.M., Ward, L.M., 2017. Unified principles of thalamo-cortical processing: the neural switch. *Biomed. Eng. Lett.* 7, 229–235.
- Robinson, S.E., 2004. Localization of event-related activity by SAM(erf). *Neurol. Clin. Neurophysiol.* NCN 2004, 109.
- Robinson, Stephen E., Vrba, Jiri, 1999. Functional neuroimaging by synthetic aperture magnetometry (SAM). *Recent Adv. Biomagn.*
- Saarinen, Timo, Jalava, Antti, et al., 2015. Task-sensitive reconfiguration of corticocortical 6–20 Hz oscillatory coherence in naturalistic human performance. *Hum. Brain Mapp.* 36 (7), 2455–2469.
- Schoffelen, Mathijs, Jan, Gross, Joachim, 2009. Source connectivity analysis with MEG and EEG. *Hum. Brain Mapp.* 30 (6), 1857–1865.
- Schoonheim, Menno M., Geurts, Jeroen J.G., et al., 2013. Functional connectivity changes in multiple sclerosis patients: a graph analytical study of MEG resting state data. *Hum. Brain Mapp.* 34 (1), 52–61.

- Sekihara, K., Hild II, K.E., et al., 2007. Adaptive spatial filter and adaptive inverse modeling for electromagnetic source imaging. In: Proc. Of 2007 Joint Meet. of the 6th Int. Symp. on Noninvasive Functional Source Imaging of the Brain and Heart and the Int. Conf. on Functional Biomedical Imaging, NFSI and ICFBI 2007.
- Sekihara, K., Nagarajan, S.S., 2008. Adaptive Spatial Filters for Electromagnetic Brain Imaging. Springer, Berlin.
- Sekihara, Kensuke, Nagarajan, Srikanth S., et al., 2002. Application of an MEG eigenspace beamformer to reconstructing spatio-temporal activities of neural sources. *Hum. Brain Mapp.* 15 (4), 199–215.
- Singer, W., 2010. Temporal coherence: a versatile code for the definition of relations. In: *The Senses: A Comprehensive Reference*, vol. 2, pp. 1–9.
- Stam, Cornelis J., Guido, Nolte, et al., 2007. Phase lag index: assessment of functional connectivity from multi channel EEG and MEG with diminished bias from common sources. *Hum. Brain Mapp.* 28 (11), 1178–1193.
- Van Veen, B.D., van Drongelen, W., et al., 1997. Localization of brain electrical activity via linearly constrained minimum variance spatial filtering. *IEEE (Inst. Electr. Electron. Eng.) Trans. Biomed. Eng.* 44 (9), 867–880.
- Vinck, M., Oostenveld, R., et al., 2011. An improved index of phase-synchronization for electrophysiological data in the presence of volume-conduction, noise and sample-size bias. *Neuroimage* 55 (4), 1548–1565.
- Vrba, Jiri, Robinson, Stephen E., 2001. Signal processing in magnetoencephalography. *Methods* 25 (2), 249–271.
- Wang, Sheng H., Lobier, Muriel, et al., 2018. Hyperedge bundling: a practical solution to spurious interactions in MEG/EEG source connectivity analyses. *Neuroimage* 173, 610–622.
- Wens, V., Marty, B., et al., 2015. A geometric correction scheme for spatial leakage effects in MEG/EEG seed-based functional connectivity mapping. *Hum. Brain Mapp.* 36 (11), 4604–4621.
- Yeo, B.T.T., Krienen, F.M., et al., 2011. The organization of the human cerebral cortex estimated by intrinsic functional connectivity. *J. Neurophysiol.* 106 (3), 1125–1165.